Analysis of gaseous ammonia (NH_3) absorption in the visible spectrum of Jupiter - Update

Patrick G. J. Irwin, Neil Bowles, Ashwin S. Braude, Ryan Garland, and Simon Calcutt

Department of Physics, University of Oxford, Parks Rd, Oxford OX1 3PU, UK.

Phillip A. Coles, Sergey N. Yurchenko and Jonathan Tennyson

Department of Physics and Astronomy, University College London, London WC1E 6BT, UK

patrick.irwin@physics.ox.ac.uk

Received _____; accepted _____

ABSTRACT

An analysis of currently available ammonia (NH_3) visible-to-near-infrared gas absorption data was recently undertaken by Irwin et al. (Icarus, 302 (2018) 426) to help interpret Very Large Telescope (VLT) MUSE observations of Jupiter from 0.48 – 0.93 μm, made in support of the NASA/Juno mission. Since this analysis a newly revised set of ammonia line data, covering the previously poorly constrained range 0.5 – 0.833 μm, has been released by the ExoMol project, "C2018" (Coles et al. 2018), which demonstrates significant advantages over previously available data sets, and providing for the first time complete line data for the previously poorly constrained 5520- and 6475-Å bands of NH_3. In this paper we compare spectra calculated using the ExoMol–C2018 data set (Coles et al. 2018) with spectra calculated from previous sources to demonstrate its advantages. We conclude that at the present time the ExoMol–C2018 dataset provides the most reliable ammonia absorption source for analysing low- to medium-resolution spectra of Jupiter in the visible/near-IR spectral range, but note that the data are less able to model high-resolution spectra owing to small, but significant inaccuracies in the line wavenumber estimates. This work is of significance not only for solar system planetary physics, but for future proposed observations of Jupiter-like planets orbiting other stars, such as with NASA's planned Wide-Field Infrared Survey Telescope (WFIRST).

Subject headings: planets and satellites: atmospheres — planets and satellites: individual (Jupiter)

1. Introduction

In a recent paper (Irwin et al. 2018) we reported an analysis of the currently available sources of gaseous ammonia (NH_3) absorption data to model observations of Jupiter we have been making with the MUSE (Multi Unit Spectroscopic Explorer, Bacon et al. (2010)) instrument at ESO's (European Southern Observatory) Very Large Telescope (VLT), in support of the NASA/Juno mission. We found that the ammonia k-tables generated from the band models of Bowles et al. (2008) provided the best combination of reliability and wavelength coverage for the MUSE spectral range, although these data were found to become very noisy at wavelengths less than 0.758 μm, leading to uncertain absorption coefficients, and did not cover the bands at 0.648 and 0.552 μm. We also found that the data of Bowles et al. (2008) seemed consistent with the ExoMol – BYTe ammonia line data of Yurchenko et al. (2011), where they overlap (0.8 - 1.05 μm), but that the existing BYTe data did not cover the ammonia absorption bands at 0.79 and 0.765 μm, which are prominent in our MUSE observations. At shorter wavelengths we found that the laboratory observations of Lutz and Owen (1980) provided a good indication of the position and shape of the ammonia absorptions near 0.552 μm and 0.648 μm, but their absorption strengths seemed inconsistent with the available data at longer wavelengths and there was no reliable way to extrapolate the strength and shape of these bands to the cold, H_2-He broadening conditions in Jupiter's atmosphere. Finally, we concluded that the line data of the 0.648-μm band of Giver et al. (1975) were not suitable for modelling these data as they accounted for only 17% of the band absorption and lacked information on lower state energies, necessary to compute their absorption strengths at low temperatures.

In this paper we compare these data sources with a newly released room temperature ammonia line list, "C2018" (Coles et al. 2018) from the ExoMol project (Tennyson and Yurchenko 2012; Tennyson et al. 2016). The new line list covers an extended wavelength

range compared to BYTe (Yurchenko et al. 2011), such that the shortest wavelength covered has been reduced from 0.833 to 0.5 μm (i.e. upper wavenumber increased from 12000 cm^{-1} to 20000 cm^{-1}) and find that the revised ExoMol line data, C2018, provide a very good and reliable resource for modelling our VLT/MUSE observations and indeed all future visible/near-IR observations of Jupiter.

2. New ExoMol ammonia line data

The previously existing ExoMol (Tennyson and Yurchenko 2012; Tennyson et al. 2016) ammonia line data set, BYTe (Yurchenko et al. 2011), contained over 1 billion lines based on an empirically-tuned potential energy surface (PES), and an *ab initio* dipole moment surface and variational nuclear motion calculations. Tuning of the PES involved adding a perturbation term to the *ab initio* surface, which is then varied through a least-squares-fitting procedure to both experimentally derived energies and *ab initio* electronic energies (Yurchenko et al. 2011). By this process the accuracy of the PES is drastically improved, whilst still retaining a form that closely resembles the *ab initio* surface.

BYTe covers the spectral range 0 – 12000 cm^{-1} (i.e. wavelengths longer than 0.833 μm), and includes line strengths and lower state energies, but does not have any information on line widths. Hence, for our previous study of available ammonia absorption data (Irwin et al. 2018), we had to undertake further analysis and assumptions and assign line widths (under H_2/He-broadening conditions) and their temperature dependences in order to apply these data to radiative transfer calculations under Jovian conditions. Most of the lines are 'hot lines' that only become important at high temperature (i.e. $T > 400$ K) and are not important at Jovian temperatures. Hence, we initially reduced the number of lines to a more manageable level by using the lower state energies and partition function to

compute the line strengths at 400 K and neglected lines contributing less than 10^{-4} % to the total line strength[1]. Once we had reduced the number of lines, we then needed to add line-broadening information since (unless the lines are to be used for calculations at low pressure and high temperature conditions, where only Doppler-broadening of the lines is important) we need information on the pressure-broadened line widths to compute the Voigt lineshape for each line. Following Amundsen et al. (2014) and Garland (2018), the foreign-broadening line widths of the NH_3 lines in a solar composition H_2-He (assumed 85:15 ratio) atmosphere were allocated from the data of Pine et al. (1993) (depending on the rotational energy level J), while the temperature-dependence exponents of these widths were taken from Nouri et al. (2004) and Sharp and Burrows (2007) for H_2-broadening and He-broadening, respectively, and used to compute a weighted-average of 0.66 (Garland 2018). For self-broadening, the line widths were taken from Markov et al. (1993) (not Pine et al. (1993) as was mistakenly reported by Irwin et al. (2018)), while the temperature dependence exponent was set to the default expected theoretical value of 0.5[2].

The newly computed room-temperature ExoMol ammonia line list, C2018 (Coles et al. 2018), covers the 0 – 20000 cm^{-1} range (i.e. wavelengths longer than 0.5 μm), and, for this work, was provided in a HITRAN-like format with line widths and temperature dependences included from a number of different sources, which are reviewed by Wilzewski et al. (2015). The H_2-broadening widths were taken from the polynomial fit by Nemtchinov et al. (2004) up to $J = 9$, and a value of 0.0788 cm^{-1} atm^{-1} assumed beyond this, as

[1]summed over 1 cm^{-1}-wide bins

[2]The collisioned-broadened width, γ, is proportional to 1/(time between collisions), or equivalently the thermal velocity divided by the mean-free-path. Since thermal velocity, $v \propto \sqrt{T}$ and mean free path, $\lambda \propto 1/\text{density}$, or equivalently $\lambda \propto T/p$, we find $\gamma \propto p/\sqrt{T}$, giving a temperature dependence exponent of 0.5.

used by Wilzewski et al. (2015). The He-broadening widths were taken from Wilzewski et al. (2015), who used the unpublished polynomial fit by Linda R. Brown up to $J = 9$ and a value of 0.0282 cm^{-1} atm^{-1} for higher J values. The self-broadening coefficients were also taken from a polynomial fit by Nemtchinov et al. (2004) up to $J = 8$, and a value of 0.5 cm^{-1} atm^{-1} assumed for higher J-values, as given in HITRAN2016 (Gordon et al. 2017). The temperature dependence of the H_2-broadening was taken from Wilzewski et al. (2015), who used the polynomial fit by Nemtchinov et al. (2004) up to $J = 9$ and a value of 0.59 thereafter. The temperature dependence of the He-broadening was estimated to be 0.37 as given by Wilzewski et al. (2015), who averaged the data from several sources. The temperature dependence of self-broadening was taken to be 0.79 by averaging the measured values of Baldacchini et al. (2000).

Compared to BYTe, the C2018 line list (Coles et al. 2018) is based on an improved, empirical potential energy surface and a significantly larger ro-vibrational basis set used in the diagonalization of the molecular Hamiltonian. These improvements are necessary for the extension to short wavelengths. Using the same spectroscopic model, a hot line list complete up to 1500 K for frequencies below 12000 cm^{-1}, and up to 300 K for the 12000−20000 cm^{-1} range (Coles et al. 2019), is under construction and will eventually contain several billion lines. This will be the full "CoYuTe" line list and, as well as being suitable for higher temperatures, will have the calculated energies replaced by their corresponding experimental values if and where possible. These energies are all below 7555 cm^{-1}, and for these lines there will be a very small improvement on some line positions (< 0.1 cm^{-1}). However, these improvements will not affect calculations in the visible/near-IR range at temperatures less than 400 K and so in the range we are considering in this paper the C2018 and CoYuTe data sets are effectively identical.

Although the room-temperature line list used here, C2018, contains far fewer lines

than the final high-temperature CoYuTe line database (Coles et al. 2019), it still comprises over 290 million lines in the 9500 - 20000 cm^{-1} range. The line strengths listed in C2018 in this spectral range are summarised in Fig. 1. This is far too large a number of lines to realistically use with current analysis techniques. As a first approximation, it is possible to eliminate all lines with a strength of less than a certain cut-off, as we did previously with the ExoMol–BYTe set (Irwin et al. 2018), and initially all lines with a strength (at 296K) of less than 1×10^{-28} cm^{-1}/(molecule cm^{-2}) were neglected, which reduced the number of lines in the 9500 - 20000 cm^{-1} spectral range to 1.3 million. Our initial test calculations were made with this table, but we were concerned whether it was reliable to simply ignore so many lines. Hence we generated two further subsets, eliminating all lines with a strength less than 1×10^{-30} and 1×10^{-32} cm^{-1}/(molecule cm^{-2}), respectively, which contained 8.8 million and 38 million lines each. Calculating test transmission spectra in the 6475 Å band (Fig. 2), we found that there were very small differences between spectra calculated with a lower strength cut-off of 1×10^{-28} and 1×10^{-30}, respectively, but negligible difference going from 1×10^{-30} to 1×10^{-32}. However, as the mean strength of the lines in C2018 reduces as we go to higher wavenumbers we were concerned that a cut-off of even 1×10^{-30} might not be suitable at shorter wavelengths. In addition, we found that the size of the database for a strength cut-off of 1×10^{-30} (nearly 9 million lines) led to excessively long computation times when converting these data to the k-tables necessary to model Jovian reflectance spectra. Hence, we looked to see whether it might be possible to more generally, reliably and efficiently model the small, but potentially significant effect of the numerous weak lines in databases such as C2018 and CoYuTe.

To do this we first of all analysed the full C2018 line database in wavenumber bins of a certain 'medium' size, which we chose to be $\Delta\tilde{\nu} = 10$ cm^{-1}. The lines in each bin were then read in and, if their strength exceeded a chosen minimum, were copied to a new database as before. However, the remaining lines, which would otherwise have been

rejected, were instead combined into a set of 'pseudo line-continuum' parameters, computed for each bin: A) $S_T(T_C) = \sum S_i(T_C)$, the sum of the line strengths for all of the omitted lines: B) $\bar{E}_l$, the line-strength-weighted mean lower state energy of the omitted lines (i.e. $\bar{E}_l = \sum S_i(T_C)E_i / \sum S_i(T_C)$); C) $\bar{\gamma}_f$, the line-strength-weighted mean foreign-broadened line width of these lines; D) $\bar{\gamma}_s$, line-strength-weighted mean self-broadened line width of these lines; E) $\bar{n}_f$, the line-strength-weighted mean temperature dependence of the foreign-broadening coefficients of these lines; and F) $\bar{n}_s$, the line-strength-weighted mean temperature dependence of the self-broadening coefficients of these lines.

When calculating the subsequent contribution of these weak lines to the continuum at wavenumber, $\tilde{\nu}$, and calculation temperature, T, we first calculated the cumulative strength of the weak lines in each bin as:

$$S_T(T) = S_T(T_C)\frac{Q_V(T_C)Q_R(T_C)(1-\exp(-E_T/kT))\exp(-\bar{E}_l/kT)}{Q_V(T)Q_R(T)(1-\exp(-E_T/kT_C))\exp(-\bar{E}_l/kT_C)} \quad (1)$$

where $Q_V(T)$ and $Q_R(T)$ are the vibration and rotation partition functions, respectively, of the gas in question, $(1-\exp(-E_T/kT))$ is a correction for stimulated emission, equal to one minus the ratio of Boltzmann populations for the two states (E_T is the transition energy, equal to $100hc\tilde{\nu}_0$, where $\tilde{\nu}_0$ is the wavenumber at the centre of the bin), and $\exp(-\bar{E}_l/kT)$ is the Boltzmann population of line-strength-weighted mean energy $\bar{E}_l$. We decided to model the effect of our pseudo line-continuum parameters not just within the individual bins themselves, but also in adjacent bins. This can be important when we have neighbouring bins containing weak lines of very different cumulative strength under conditions of considerable line broadening, where we might see the wings of the stronger lines from one bin noticeably spilling into adjacent bins with significantly lower cumulative strength. Assuming the weak lines to be equally distributed throughout the bin, n, with central wavenumber $\tilde{\nu}_n$, we calculate the contribution of these absorptions in a neighbouring

bin, i, with central wavenumber, $\tilde{\nu}_i$, to be

$$C_{ni}(T) = \frac{S_n(T)V(x_{ni}, y)}{\sum_i V(x_{ni}, y)} \tag{2}$$

where $V(x_{ni}, y)$ is the line-shape function (usually Voigt, including or excluding line wing corrections), $x_{ni} = \tilde{\nu}_i - \tilde{\nu}_n$, and $y = \gamma_L/\gamma_D$, where, assuming foreign-broadened conditions, the pressure-broadening line width is

$$\gamma_L = \bar{\gamma}_f \frac{p}{p_C} \left(\frac{T_C}{T} \right)^{\bar{n}_f} \tag{3}$$

and the Doppler-broadened line width is

$$\gamma_D = \frac{\tilde{\nu}_0}{c} \left(\frac{2RT}{M_r} \right)^{1/2} \tag{4}$$

where M_r is the Molecular Weight of the gas in question. These pseudo line-continuum contributions are then added and the mean continuum absorption at each bin centre calculated to be:

$$\bar{k}_n(T) = \sum_i C_{ni}(T)/\Delta\tilde{\nu} \tag{5}$$

We show this process graphically in Fig. 3, where we focus on five adjacent bins of width $\Delta\tilde{\nu} = 10$ cm^{-1}; here we have arbitrarily set different cumulative weak line strengths in the bins, indicated by the coloured horizontal lines. The contribution to the continuum absorption of the lines in one bin to the same bin and adjacent bins (within any line wing cutoff) is computed using the required line shape and the calculated values at the bin centres normalised to ensure they sum to the integrated line strength in the original bin. The total contribution at the bin centres from the bin itself and adjacent bins is then added and these values interpolated to determine the final continuum spectrum. We find that using these equations to calculate the contribution of the lines that were previously simply discarded gives excellent correspondence with calculations that omit no lines at temperatures close to T_C, but discrepancies can arise as $|T - T_C|$ becomes greater. Hence,

since our k-tables are calculated over a wide range of temperatures, we computed pseudo line-continuum parameters at each k-table temperature separately, thus avoiding entirely this temperature extrapolation error.

Finally, we also explored using the same system to assign to the 'pseudo line continuum' lines that were not amongst the top N strongest lines in the bin, or lines contributing less than a certain minimum percentage of the total integrated line strength. This may prove eventually to be more efficient and adaptable than simply assigning all lines with a strength less than a certain cut-off line strength, as we have done here, but development issues led us to use the simpler minimum strength cut-off system described here. We may return to a more general approach in future work.

Taking the C2018 line database, we computed a set of reduced line databases and pseudo line-continuum tables (in 10 cm^{-1}-wide bins) at a range of temperatures equally spaced between 50 and 400K with a cut-off line strength at each calculation temperature of 1×10^{-28} cm^{-1}/(molecule cm^{-2}). These line databases and continuum tables were then used to compute k-distribution look-up tables to model our VLT/MUSE observations for H_2-He-broadening conditions (assuming H_2:He = 0.865:0.135), covering the spectral range 0.4 – 1.0 μm. These k-tables are used in our correlated-k radiative transfer model, NEMESIS, described later. In these k-tables, 10 g-ordinates were used with 15 pressures logarithmically spaced between 10^{-4} and 10 bar and the 20 temperatures, mentioned before, equally spaced between 50 and 400K.

3. Comparison with Lutz and Owen (1980) and Giver (1975) absorption data

Lutz and Owen (1980) report room-temperature laboratory measurements of the absorption spectrum of NH_3 for both the 6475 Å band and the 5520 Å band at a quoted

spectral resolution of 2 Å. These data are presented in the form of apparent absorption cross-sections. We found in our previous analysis (Irwin et al. 2018) that these data provided a good estimate of the shape of the 6475 Å and 5520 Å bands in the observed VLT/MUSE observations, but that the estimated strengths under Jovian conditions were not consistent with the strength of ammonia gas absorption features calculated at longer wavelengths with line data. We attributed this discrepancy to the fact that Lutz and Owen (1980) report observations under self-broadened conditions, rather than H_2–He-broadened conditions, and only for a single temperature with no simple means to extrapolate to lower temperatures.

In addition, we analysed line data extracted from low- and high-resolution (R= $\lambda/\Delta\lambda = 170,000$) laboratory spectra of self-broadened ammonia in the 6475 Å band at room temperature by Giver et al. (1975). In this line database the strengths of the thirty three strongest lines in the 6475 Å band were estimated as were their self-broadened linewidths. For our analysis of these data we assigned the H_2-He-broadened linewidth for all lines to be 0.101 cm^{-1}, which is an average of the H_2-broadened linewidths of lines in this band reported by Keffer et al. (1985, 1986). However, a key drawback of these data is that they are derived from room temperature observations only and thus do not include an estimate of the lower state energy of the lines. Hence, it is again difficult to use these data to model the infrared spectrum of cold planets such as Jupiter or hot exoplanets since we cannot compute how the strengths vary with temperature.

Fig. 4 shows a 'low dispersion' spectrum of a laboratory path of ammonia measured by Giver et al. (1975), where we hand-digitised the spectrum shown in their Fig.3 and which we previously showed in Fig. 2 of Irwin et al. (2018). The path was 36 m long and contained 1 atm pressure of pure ammonia at a temperature of 294 K. In Fig. 4 we compare the measured spectrum with that calculated using the new ExoMol–C2018 line data (Coles

et al. 2018), where we found that smoothing the line-by-line calculated spectrum to a spectral resolution of R = 3000 (i.e. 2.15 Å) provided the best correspondence to the measured Giver et al. spectrum. In Fig. 4 we also show the corresponding spectrum calculated with the cross-section data of Lutz and Owen (1980). The resolution of these data is quoted as 2 Å by Lutz and Owen (1980), but when we smoothed our line-by-line calculated spectrum to this resolution we found poor correspondence. Instead, in Fig. 4, we smoothed the C2018-calculated line-by-line spectrum to a resolution of 10 Å , which we found provided a reasonable match to the resolution of the spectrum calculated with the Lutz&Owen data, and conclude that the true resolution of the Lutz&Owen data is actually 10 Å, not 2 Å.

It is clear from Fig. 4 that the ExoMol–C2018 ammonia line data (Coles et al. 2018) provide a reasonable correspondence, given the uncertainties in line positions of the ExoMol line data, with the self-broadened laboratory measurements of Giver et al. (1975) and Lutz and Owen (1980) for the 6475 Å band. We also looked to see how well these data matched the data of Lutz and Owen (1980) for the 5520 Å band (this band was not measured by Giver et al. (1975)). Figure 5 shows the spectrum of the 5520 Å band calculated for the same path length and conditions as Fig. 4 using the Lutz and Owen (1980) data. Overplotted in Fig. 5 is the spectrum calculated with the C2018 line data, smoothed to a resolution of 1.8 Å (i.e. R = 3000) and 10 Å, respectively. We find that the lower resolution calculated spectrum provides a reasonable match to the Lutz&Owen spectrum, but that there are differences in the calculated position of the longer-wavelength absorption peak. It is not clear whether this discrepancy arises from: 1) errors in digitising the Lutz&Owen data; 2) errors in the wavelength scale of the published Lutz&Owen data; or 3) errors in the line positions in the C2018 line data (Coles et al. 2018). In particular, the potential energy surface used to construct the line list was only tuned to energy levels below 10,000 cm^{-1} and can therefore be expected to become increasingly inaccurate for wavelengths

shorter than 1 μm. However, we also note that there appears to be a discrepancy between Figs. 1 and 4 of Lutz and Owen (1980). In Fig. 1 of Lutz and Owen (1980), the shorter wavelength absorption peak is clearly at a wavelength less than 5500 Å and the second peak at a wavelength least 25 Å longer. However, in their Fig. 4, it appears that there is only a 56 cm^{-1} difference between the peaks, which equates to a 17 Å difference. Hence, it may be that there are indeed errors in the wavelength scale of the published Lutz&Owen data.

To compare the line data of the ExoMol–C2018 line database with the measurements in more detail, we hand-digitised the published high-resolution (quoted spectral resolving power R $\sim$ 170,000) laboratory spectra of Giver et al. for the 6475 Å band (shown as Fig.1 of Giver et al. 1975) for a low pressure path of length 400m, pressure 0.061 atm and temperature 294K. Giver et al. (1975) showed these spectra spread over three pages and we repeat this format here, comparing our digitised version with line-by-line-calculated spectra in Figs 6 – 8. We find that spectra calculated[3] with the line data of Giver et al. (1975) have absorption lines that match the position and strength of many of the stronger measured lines, for example at 6449.95 Å and 6457.05 Å, but that many are not represented; this is entirely as expected since these line data were only published for the thirty-three strongest lines. Spectra calculated from the ExoMol–C2018 line data match better the overall distribution of different line strengths, (i.e. that in broad wavelength intervals the ExoMol lines are weak where the measured lines are weak, and the ExoMol lines are strong where the measured lines are strong) but the line centres do not match the

[3]N.B. We found that our line-by-line spectra had to be smoothed to a resolution of 0.06 Å to provide best correspondence with the observed spectra, which indicates that the actual spectral resolution of the high resolution observations was $\sim$108,000, rather than $\sim$170,000 as quoted by Giver et al. (1975)

individual observed line positions very well at all. The generally good agreement of the ExoMol lines with broad distribution of observed absorption lines can be seen more clearly in Fig. 9, where the measured absorption spectrum is compared with the calculated spectra over the entire 6418 – 6548 Å wavelength range at three different spectral resolutions: 0.06 Å(i.e. original resolution), 1.0 Å and 10.0 Å (all assuming a triangular line shapes). We can see that the spectra calculated with the ExoMol line data reproduce the overall shape of the absorption band well at lower resolution, but predict slightly more absorption and also predict that the wavelengths of peak absorption occur at slightly longer wavelengths than those observed (5 – 10 Å). The same comparisons can be drawn when comparing the spectra observed/calculated for the higher pressure path shown in Fig. 4. At high resolution, the poor correspondence between the observed and predicted line centres, but better correspondence between the observed and predicted line strengths is not surprising since at shorter wavelengths we expect these computed data to be more accurate in predicting the strengths of different absorption lines than their line positions. Owing to the lack of empirically-derived energies below 1 μm at the time of producing the PES used by Coles et al. (2018), line positions below 1 μm may be several, or even tens of wavenumbers in error depending on the upper state vibrational mode and J. These inaccuracies are discussed by Zobov et al. (2018) in their analysis of the red and green optical spectrum of ammonia. Hence, we conclude that the ExoMol–C2018 line data provide a very useful resource for modelling low- to medium-resolution observed spectra, but should be used with caution when analysing high-resolution observations.

4. Comparison with Bowles et al. (2008) absorption data

Bowles et al. (2008) report Goody-Lorentz band models fitted to the measured absorption spectra of laboratory paths of ammonia with path lengths of 2.164 and 10.164

m, pressures ranging from 0.075 to 1.02 bar and temperatures varying between 216 and 292 K. The measured transmission spectra cover the spectral range 0.74 - 1.0475 μm and have a spectral resolution and step of 0.0025 μm. Irwin et al. (2018) found that the band data of Bowles et al. (2008) become increasingly noisy at shorter wavelengths. The shortest wavelength absorptions were only visible at the longest path lengths, highest pressures and highest temperatures in the laboratory measurements and these features were essentially lost in the noise at lower temperatures. This is because at lower temperatures, since the pressure cannot be allowed to exceed the saturated vapour pressure of ammonia (to avoid condensation on the surfaces of the experiment) this necessarily limits the path amounts that can be attained. Figure 10 shows the laboratory spectra measured by Bowles et al. (2008) at the longest available path lengths for four temperatures in the range 215 – 295 K (shown as Fig. 4 in Irwin et al. (2018)), together with simulated spectra for the same paths calculated with the ExoMol–C2018 line data (line-by-line) for self-broadened conditions and then smoothed to the resolution of the Bowles et al. (2008) data, i.e. 0.0025 μm. As can be seen there is an excellent correspondence between the measured spectra and the ExoMol–C2018 calculations, with mean transmission differences of 0.015, increasing to 0.15 at the very longest wavelength. However, the ExoMol–C2018 (Coles et al. 2018) line data has a much better, smoother variation at the shorter wavelengths, where the Bowles data was found by Irwin et al. (2018) to become unreliable.

5. Analysis of MUSE observations

Figure 11 shows a typical spectrum of Jupiter extracted from our MUSE observations (Braude et al. 2019) from 9th April 2018 from a single pixel in the Equatorial Zone near the sub-Earth point and similar to the spectrum observed on 28th May 2017 shown as Fig. 9 of Irwin et al. (2018). As before the MUSE spectra were smoothed with a

triangular line shape of FWHM=0.002 μm, and sampled with a step of 0.001 μm, giving a spectral resolution of $R \sim 250$. Similarly, as in our previous analysis, these spectra were modelled with our NEMESIS (Irwin et al. 2008) radiative transfer and retrieval tool, using the method of correlated-k (e.g. Lacis and Oinas (1991)) in its radiative transfer scheme, and modelling multiple scattering using the matrix-operator method of Plass et al. (1973). The absorption of ammonia gas was modelled using either the band data of Bowles et al. (2008), converted to k-tables as described by Irwin et al. (2018), together with the Lutz and Owen (1980) cross-sections for the 0.55 and 0.65 μm ammonia absorption bands (with no temperature dependance assumed), or using the new k-tables generated from the ExoMol–C2018 line list (Coles et al. 2018), described earlier. Methane absorption was modelled with a k-table generated from the band data of Karkoschka and Tomasko (2010), while small absorption features from H_2 lines were modelled with a k-table generated from line data from the HITRAN 2012 line database (Rothman et al. 2013). The collision-induced absorption of H_2–H_2 and H_2–He at these wavelengths was modelled after Borysow et al. (1989a,b, 2000), while at shorter wavelengths, the Rayleigh-scattering opacity was modelled via standard theory (e.g. Goody and Yung 1989; Hansen and Travis 1974), accounting for the contributions of H_2, He, CH_4 and NH_3. For this reflectance calculation, the observed radiances were divided by a reference solar spectrum, using Jupiter's distance from the sun of 5.42 AU on this date. For this, the solar spectrum of Chance and Kurucz (2010) was used, which was first smoothed with a triangular line shape of FWHM = 0.002 μm to make it compatible with our smoothed spectra.

Figure 11 shows our best fit to the Equatorial Zone spectrum using the combined Bowles et al. and Lutz&Owen data, and then the fit resulting from using the NH_3 k-table generated from the ExoMol–C2018 line list (Coles et al. 2018). Figure 12 shows the same comparison for a spectrum measured in the North Equatorial Belt (corresponding to Fig. 10 of Irwin et al. (2018)).

As can be seen we are able to fit the VLT/MUSE observations of the EZ and NEB significantly better with the ExoMol–C2018 NH_3 absorption data than we can using our previous best combination of the data of Bowles et al. (2008) and Lutz and Owen (1980). The χ^2/n of the fit was reduced from 1.93 to 1.60 for the EZ, and from 2.06 to 1.76 for the NEB. Our previous list of visible NH_3 'features' are marked in Figs. 11 and 12 as: A – 0.552 μm, B – 0.648 μm, C – 0.75 μm, D – 0.765 μm, E – 0.79 μm, F – 0.825 μm and G – 0.93 μm. It can be seen that the feature 'C' now appears to be an artefact of the data of Bowles et al. (2008), but the others seem real and are clearly very well fit simultaneously using the ExoMol–C2018 line data. We should also that feature 'D' at 0.765 μm coincides almost exactly with an O_2-absorption band in the telluric spectrum. This appears to have been incompletely corrected for in the spectrum from 2017 shown by Irwin et al. (2018), which made the discrepancy at this wavelength look worse. For the spectrum presented here (from 2018) where a more reliable telluric correction was achieved, feature 'D' is much less pronounced and seems equally well fit by the ExoMol–C2018 and Bowles et al. data. However, in summary, it can be seen that over the whole MUSE spectral range, the new ExoMol–C2018 line data for NH_3 (Coles et al. 2018) greatly improve our ability to model the near-infrared spectrum of Jupiter.

6. Conclusion

The ExoMol–C2018 NH_3 line list of Coles et al. (2018) clearly represents a significant step forward in allowing the accurate modelling of ammonia absorption in the visible/near-IR spectra of giant planets. However, while the ExoMol–C2018 data is shown to reproduce low to medium resolution features well ($R \sim 250$ and below), it is clear that the accuracy to which the wavelengths of individual lines are predicted needs to be improved for high resolution studies. It is possible to do this *post hoc* (e.g. Barber et al. (2014)), provided

346 either high-resolution measured frequencies or empirical energy levels are obtained. High
347 resolution laboratory spectroscopy studies of ammonia have long been available, e.g.
348 Lehmann and Coy (1988); however, coverage remains fragmentary and analysis of these
349 spectra difficult, as noted by Zobov et al. (2018). New laboratory studies in this region
350 would be welcome and would facilitate further improvement of the available line lists.

351 ## 7. Acknowledgements

352 The VLT/MUSE observations were performed at the European Southern Observatory
353 (ESO), proposals: 095.C-0149, 096.C-0173, 098.C-0035, 099.C-0192 and 101.C-0097.
354 We thank Larry Sromovsky for kindly providing the code we used to generate our
355 Rayleigh-scattering opacities, Renyu Hu, for providing an electronic version of the line data
356 of (Giver et al. 1975) and advising on the use of the linewidths of Keffer et al. (1985)
357 and Keffer et al. (1986), and Sergi Hildebrandt and Margaret Turnbull (WFIRST Science
358 Investigation Team PI) for coordinating the WFIRST Exoplanet Data Challenge, through
359 which these discrepancies in ammonia absorption coefficients came to light. We would also
360 like to thank our anonymous reviewers for their very detailed and helpful reviews. The work
361 at University College London was supported by the UK Engineering and Physical Sciences
362 Research Council (EPSRC) grant EP/M506448/1 and Servomex Ltd, the use of the UCL
363 Legion High Performance Computing Facility (Legion@UCL), along with the STFC DiRAC
364 HPC Facility supported by BIS National E-infrastructure capital grant ST/J005673/1 and
365 STFC grants ST/H008586/1, ST/K00333X/1.

366 *Facilities:* VLT (MUSE).

REFERENCES

Amundsen D. S., Baraffe I., Tremblin P., Manners J., Hayek W., Mayne N. J., Acreman D. M., 2014. Accuracy tests of radiation schemes used in hot Jupiter global circulation models. A&A, 564, A59.

Bacon, R., et al., 2010. The MUSE second-generation VLT instrument. Proc. SPIE 7735, Ground-based and Airborne Instrumentation for Astronomy III, 773508, doi:10.1117/12.856027.

Baldacchini, G., Buffa, G., D'Amato, F., Tarrini, O., De Rosa, M., Pelagalli, F., 2000. New results for the temperature dependence of self-broadening and shift in the ν_2 ammonia band. J. Quant. Spec. Radiat. Transf., 67, 365 – 374. doi:10.1016/s0022-4073(99)00239-3.

Barber, R.J., Strange, J., Hill, C. Polyansky, O.L., Mellau, G.N, Yurchenko, S.N., Tennyson, J., 2015. ExoMol Molecular linelists: III An improved hot rotation-vibration line list for HCN and HNC, MNRAS, 437, 1828 – 1835.

Borysow, A., Frommhold, L., Moraldi, M., 1989a. Collision-induced infrared spectra of H_2-He pairs involving $0 \rightarrow 1$ vibrational transitions and temperatures from 18 to 7000K. ApJ 336, 495 – 503.

Borysow, A., Frommhold, L.,1989b. Collision-induced infrared spectra of H_2-He pairs at temperatures from 18 to 7000K. Overtone and hot bands. ApJ ,341, 549 – 555.

Borysow, A., Borysow, J., Fu, Y., 2000. Semi-empirical model of collision-induced absorption spectra of H_2–H_2 complexes in the second overtone band of Hydrogen at temperatures from 50 to 500 K. Icarus, 145, 601–608.

Bowles, N., Calcutt, S., Irwin, P., Temple, J., 2008. Band parameters for self-broadened ammonia gas in the range 0.74 to 5.24 μm to support measurements of the atmosphere of the planet Jupiter. Icarus, 196, 612 – 624.

Braude, A.S., Irwin, P.G.J., Orton, G.S., Fletcher, L.N., 2019. Colour and tropospheric cloud structure of Jupiter from MUSE/VLT: Retrieving a universal chromophore. Icarus, (to be submitted).

Chance, K., Kurucz, R.L. 2010. An improved high-resolution solar reference spectrum for earth's atmosphere measurements in the ultraviolet, visible, and near infrared. J. Quant. Spec. Radiat. Transf., 111, 1289 – 1295.

Coles, P.A., Ovsyannikov, R.I., Polyansky, O.L., Yurchenko, S.N., Tennyson, J., 2018. Improved potential energy surface and spectral assignments for ammonia in the near-infrared region. J. Quant. Spec. Radiat. Transf., 219, 199 – 212. doi:10.1016/j.jqsrt.2018.07.022

Coles, P.A., Yurchenko, S.N., Tennyson, J., 2019. An improved variationally computed line list for hot NH_3. MNRAS (to be submitted).

Lehmann, K.K., Coy, S.L., 1988. Spectroscopy and intramolecular dynamics of highly excited vibrational states of NH_3. J. Chem. Soc. Faraday Trans. II, 84, 1389 – 1406.

Garland, R., Modelling the spectra of Brown Dwarfs. D.Phil. Thesis, University of Oxford. 2018.

Gordon, I.E. et al., 2017. The HITRAN 2016 molecular spectroscopic database. J. Quant. Spec. Radiat. Transf., 203, 3 – 69. doi:10.1016/j.jqsrt.2017.06.038.

Goody, R.M., Yung, Y.L., 1989. Atmospheric Radiation. Theoretical Basis (2nd Edition). Oxford University Press.

Giver, L.P., Miller, J.H., Boese, R.W., 1975. A laboratory atlas of the $5\nu_1$ NH_3 absorption band at 6475Å with applications to Jupiter and Saturn. Icarus, 25, 34 – 48.

Hansen, J.E., Travis, L.D., 1974. Light scattering in planetary atmospheres. Space Science Rev., 16, 527 – 610.

Irwin, P.G.J., Teanby, N.A., de Kok, R., Fletcher, L.N., Howett, C.J.A., Tsang, C.C.C., Wilson, C.F., Calcutt, S.B., Nixon, C.A., Parrish, P.D., 2008. The NEMESIS planetary atmosphere radiative transfer and retrieval tool. J. Quant. Spec. Radiat. Transf., 109, 1136 – 1150.

Irwin, P.G.J., Bowles, N., Braude, A.S., Garland, R., Calcutt, S., 2018. Analysis of gaseous ammonia (NH_3) absorption in the visible spectrum of Jupiter. Icarus, 302, 426 – 436.

Karkoschka, E., Tomasko, M.G., 2010. Methane absorption coefficients for the jovian planets from laboratory, Huygens, and HST data. Icarus, 205, 674 – 694.

Keffer, C. E., Conner, C.P, Smith, W.H., 1985. Hydrogen broadening of vibrational-rotational transitions of ammonia lying near 6450Å. J. Quant. Spec. Radiat. Transf., 33, 193 – 196.

Keffer, C. E., Conner, C.P, Smith, W.H., 1986. Pressure broadening of ammonia lines in the 6475Å band at room and low temperatures. J. Quant. Spec. Radiat. Transf., 35, 487 – 493.

Lacis, A.A., Oinas, V., 1991. A description of the correlated-k distribution method for modelling nongray gaseous absorption, thermal emission, and multiple scattering in vertically inhomogeneous atmospheres. J. Geophys. Res., 96, 9027 – 9063.

Lutz, B.L., Owen, T., 1980. The visible bands of Ammonia: Band strengths, curves of growth, and the spatial distribution of Ammonia on Jupiter. ApJ, 235, 285 – 293.

435 Markov, V.N., Pine, A.S., Buffa, G., Tarrani, O., 1993. Self broadening in the ν_1 band of
436 NH_3. J. Quant. Spec. Radiat. Transf., 50, 167 – 178.

437 Nemtchinov, V., Sung, K., Varanasi, P., 2004. Measurements of line intensities and
438 half-widths in the 10-μm bands of $^{14}NH_3$. J. Quant. Spec. Radiat. Transf., 83, 243 –
439 265. doi:10.1016/s0022-4073(02)00354-0.

440 Nouri, S., Orphal J., Aroui H., Hartmann J.-M., 2004. Temperature dependence of pressure
441 broadening of NH_3 perturbed by H_2 and N_2. J. Mol. Spec., 227, 60 – 66.

442 Pine, A., Markov V., Buffa G., Tarrini, O., 1993. N_2, O_2, H_2, Ar and He broadening in the
443 ν_1 band of NH_3, J. Quant. Spec. Radiat. Transf., 50, 337 – 348.

444 Plass, G.N., Kattawar, G.W., Catchings, F.E., 1973. Matrix operator method of radiative
445 transfer. 1: Rayleigh scattering. Appl. Opt., 12, 314 – 329.

446 Rothman, L.S., Gordon, I.E., Babikov, Y., Barbe, A., Benner, D.C., Bernath, P.F., et al,
447 2013. The HITRAN 2012 molecular spectroscopic database, J. Quant. Spec. Ra-
448 diat. Transf., 130, 4 – 50.

449 Sharp, C. M., Burrows A., 2007. Atomic and molecular opacities for brown dwarf and giant
450 planet atmospheres, ApJS, 168, 140 – 166.

451 Tennyson, J., Yurchenko, S.N., 2012. The ExoMol database: molecular line lists for
452 exoplanet and other hot atmospheres, MNRAS, 425, 21 – 33.

453 Tennyson, J., Yurchenko, S.N., Al-Refaie, A.F., Barton, E.J., Chubb, K.L, Coles, P.A,
454 et al., 2016. ExoMol: molecular line lists for exoplanet and other atmospheres, J.
455 Molec. Spectrosc., 327, 73 – 94.

456 Wilzewski, J.S., Gordon, I.E., Kochanova, R.V., Hill, C., Rothman, L. S., 2015. H_2, He,
457 and CO_2 line-broadening coefficients, pressure shifts and temperature-dependence

458 exponents for the HITRAN database. Part 1: SO_2, NH_3, HF, HCl, OCS and C_2H_2.
459 J. Quant. Spec. Radiat. Transf., 168, 193 – 206. doi:10.1016/j.jqsrt.2015.09.003.

460 Yurchenko, S.N., Barber, R.J., Tennyson, J., Thiel, W., Jensen, P., 2001 Towards efficient
461 refinement of molecular potential energy surfaces: Ammonia as a case study. J.
462 Molec. Spectrosc., 268, 123–129. doi:10.1016/j.jms.2011.04.005.

463 Yurchenko, S.N., Barber, R.J., Tennyson, J., 2011. A variationally computed line list for
464 hot NH_3, MNRAS, 413, 1828 – 1834.

465 Yurchenko, S.N., Tennyson, J., Bailey, J., Hollis, M.J.D., Tinetti, G., 2014 Spectrum of hot
466 methane in astronomical objects using a comprehensive computed line list. Proc.
467 Nat. Acad. Sci., 111, 9379 – 9383.

468 Zobov, N.F., Coles, P.A., Ovsyannikov, R.I., Kyuberis A.A., Hargreaves, R.J., Bernath,
469 P.F., et al., 2018. Analysis of the red and green optical absorption spectrum of gas
470 phase ammonia. J. Quant. Spec. Radiat. Transf., 209, 224 – 231.

This manuscript was prepared with the AAS LaTeX macros v5.2.

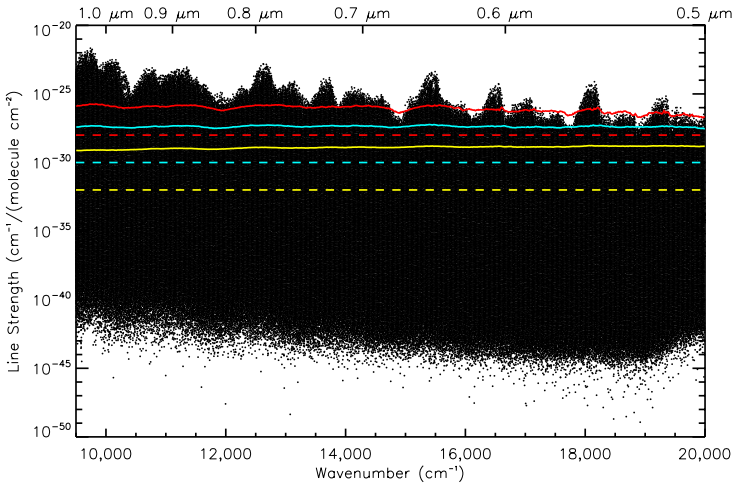

Fig. 1.— Summary of lines in the ExoMol–C2018 line database (Coles et al. 2018). The strengths of all lines (at 296 K) are shown between 9500 and 20000 cm^{-1}. Equivalent wavelengths are indicated on the top axis. The horizontal, dashed lines indicate the different line strength cut-offs that were explored of 1×10^{-28}, 1×10^{-30} and 1×10^{-32} cm^{-1}/(molecule cm^{-2}), respectively. The corresponding solid lines show the integrated 'pseudo continuum' absorption of all the omitted lines for the different cut-off strengths.

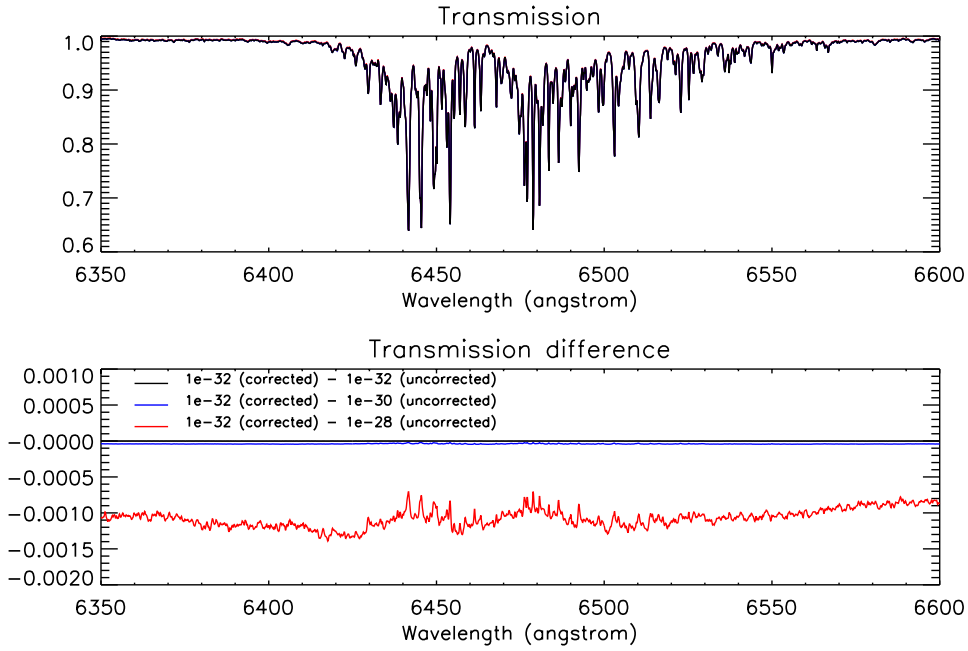

Fig. 2.— Line-by-line-calculated transmission spectrum of the self-broadened path of ammonia shown in Fig. 3 of Giver et al. (1975), with spectral resolution of 0.2Å, using the new ExoMol–C2018 linedata (Coles et al. 2018). In this calculation the temperature is 294 K, the path length is 36 m and the pressure is 1 atm. The top plot compares the calculated spectra using a line strength cut-off of 1×10^{-32} cm^{-1}/(molecule cm^{-2}) including 'pseudo line-continuum' correction (black) with spectra calculated with no line continuum correction and higher line strength cutoffs of 1×10^{-30} (blue) and 1×10^{-28} (red), respectively. As can be seen the transmission calculated with a cut-off of 1×10^{-28} and no continuum correction can just be differentiated from the other calculated spectra. The bottom plot compares the difference spectra calculated with different line strength cut-offs, including or excluding the continuum correction. Significant differences are seen for a cut-off of 1×10^{-28} cm^{-1}/(molecule cm^{-2}), but very small difference is seen for $1 \times 10^{-30}$and effectively no difference seen for 1×10^{-32}, when the continuum correction is omitted.

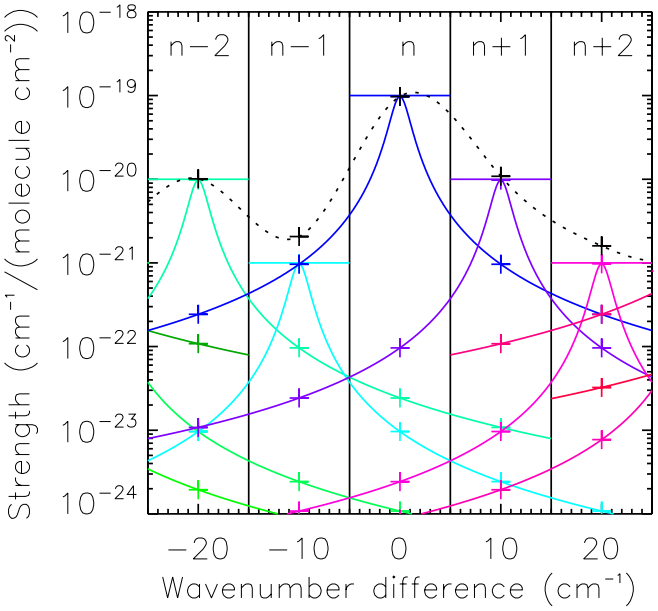

Fig. 3.— Suggested 'pseudo line-continuum' correction to deal with very large number of weak lines present in line databases such as ExoMol–CoYuTe (Coles et al. 2019). Here we focus on five adjacent bins of width 10 cm^{-1} and have arbitrarily set widely varying strengths to demonstrate the principle of the suggested scheme. The coloured, horizontal lines indicate the assigned integrated line strengths in each bin. The contribution of these lines to the continuum absorption in adjacent bins is computed using the line shape required and indicated by the coloured solid lines. Here, for simplicity, we have assumed a Lorentz line shape with FWHM = 1 cm^{-1}. We have also assumed a line wing cut-off of 35 cm^{-1}. For each bin we calculate the contribution to other bins within the line wing cut-off at the bin centres and then normalise to ensure these contributions sum to equal the integrated line strength in the original bin; the value at the bin centres are shown by the coloured crosses. The sum of contributions at each bin centre is then added to give the total in each bin indicated by the black crosses. A cubic spline is then fitted to the integrated log line strengths to allow smooth interpolation across the wavenumber. When calculating the continuum absorption in a spectrum these adjusted line strengths need to be divided by the width of the bin, here 10 cm^{-1}, to turn them into absorption coefficients.

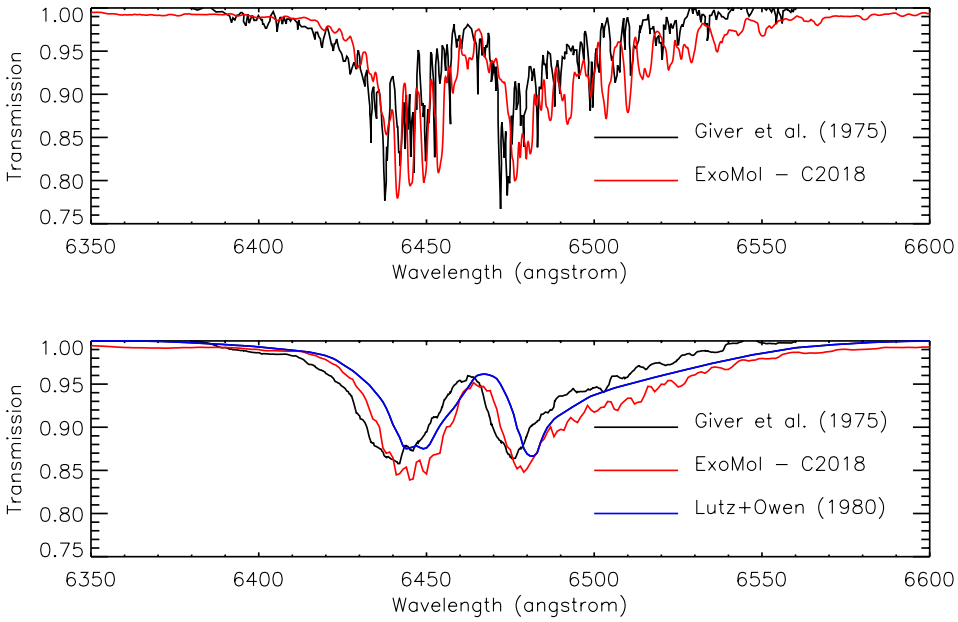

Fig. 4.— Top: Transmission spectrum of the self-broadened path of ammonia shown in Fig. 3 of Giver et al. (1975). In this calculation the temperature is 294 K, the path length is 36 m and the pressure is 1 atm. The originally measured 'low-dispersion' spectrum of Giver et al. (1975) (digitised by the authors) is shown in black. The red line in this panel shows the spectrum calculated using the new ExoMol–C2018 line data of Coles et al. (2018). The resolving power of this spectrum was not stated, but we found that if we set it to R = 3000 (i.e. dλ = 2.15 Å) we achieved reasonably good correspondence with the observed spectrum, although the line centres do not always align. Bottom: Transmission spectrum of the same self-broadened path of ammonia calculated using the absorption coefficients of Lutz and Owen (1980) (blue line). The authors claim these coefficients have a resolution of 2 Å (or 0.0002 μm), but comparing with spectra calculated using the new ExoMol–C2018 line data of Coles et al. (2018), we find that a smoothing the ExoMol data with a square function of full-width-half maxium (FWHM) of 10 Å (red line) gives a spectrum that compares much more favourably with that calculated with the coefficients of Lutz and Owen (1980). In this bottom plot we also show the 'low-dispersion' spectrum of Giver et al. (1975) smoothed to the same resolution of 10 Å (black) for reference.

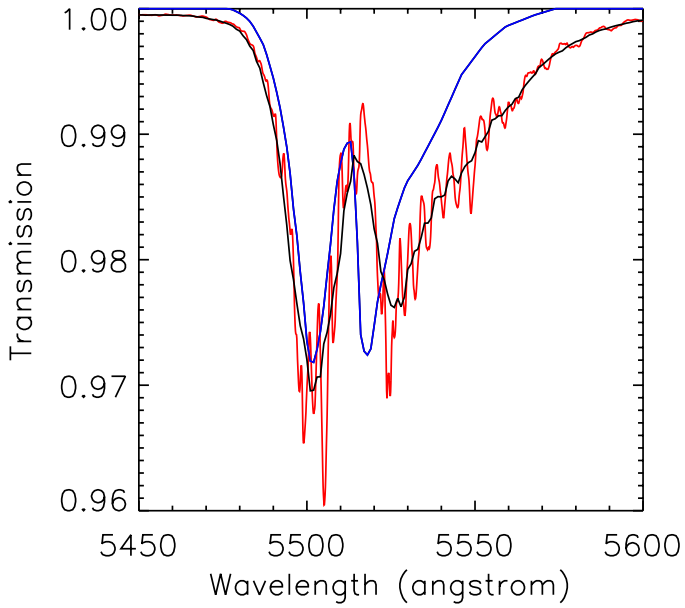

Fig. 5.— Calculated transmission for the same path computed in Fig. 4, but centred on the absorption band at 5520 Å. The blue line is the spectrum calculated using the Lutz and Owen (1980) absorption coefficients. The red line is the spectrum calculated with the ExoMol–C2018 line data (Coles et al. 2018), smoothed to a spectral resolving power of 3000 (i.e. $d\lambda = 1.8$Å), while the black line is the same spectrum smoothed to a resolution of 10 Å, which is the believed resolution of the Lutz&Owen data.

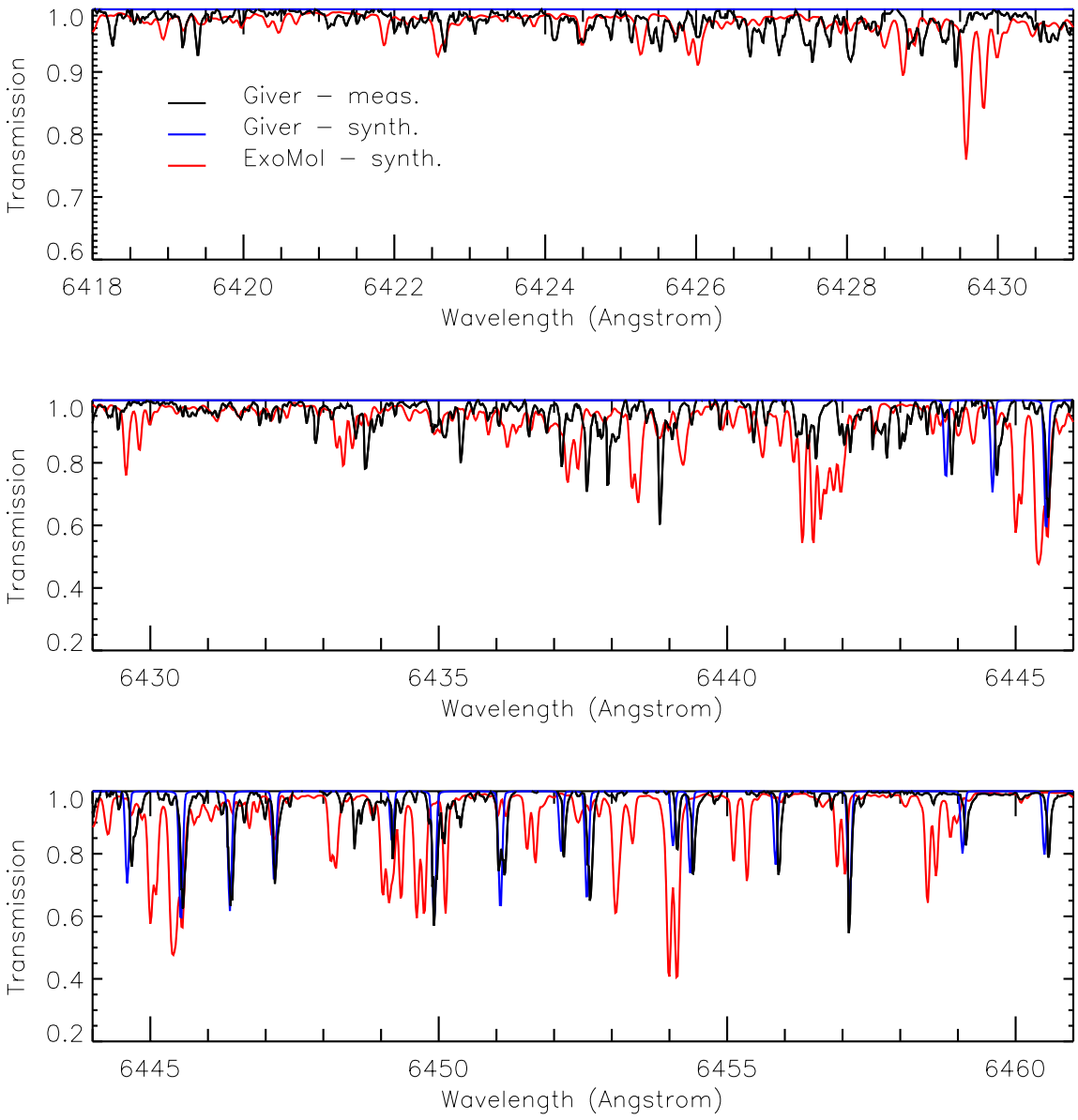

Fig. 6.— Comparison of high resolution spectra of Giver et al. (1975) (their Fig. 1) with high spectral resolution line-by-line calculations using the line data of Giver et al. (1975) and ExoMol–C2018 (Coles et al. 2018) for the conditions specified in Fig. 1. of Giver et al. (1975), i.e. length = 400m, p = 0.061 atm, T = 294 K. Here the black lines are the observed spectra in the different spectral ranges (digitised by the authors), the blue lines are the spectra calculated from the Giver et al. line data, while the red lines are the spectra calculated from the ExoMol–C2018 line data. Here the three spectra cover the spectral range 6418–6460 Å.

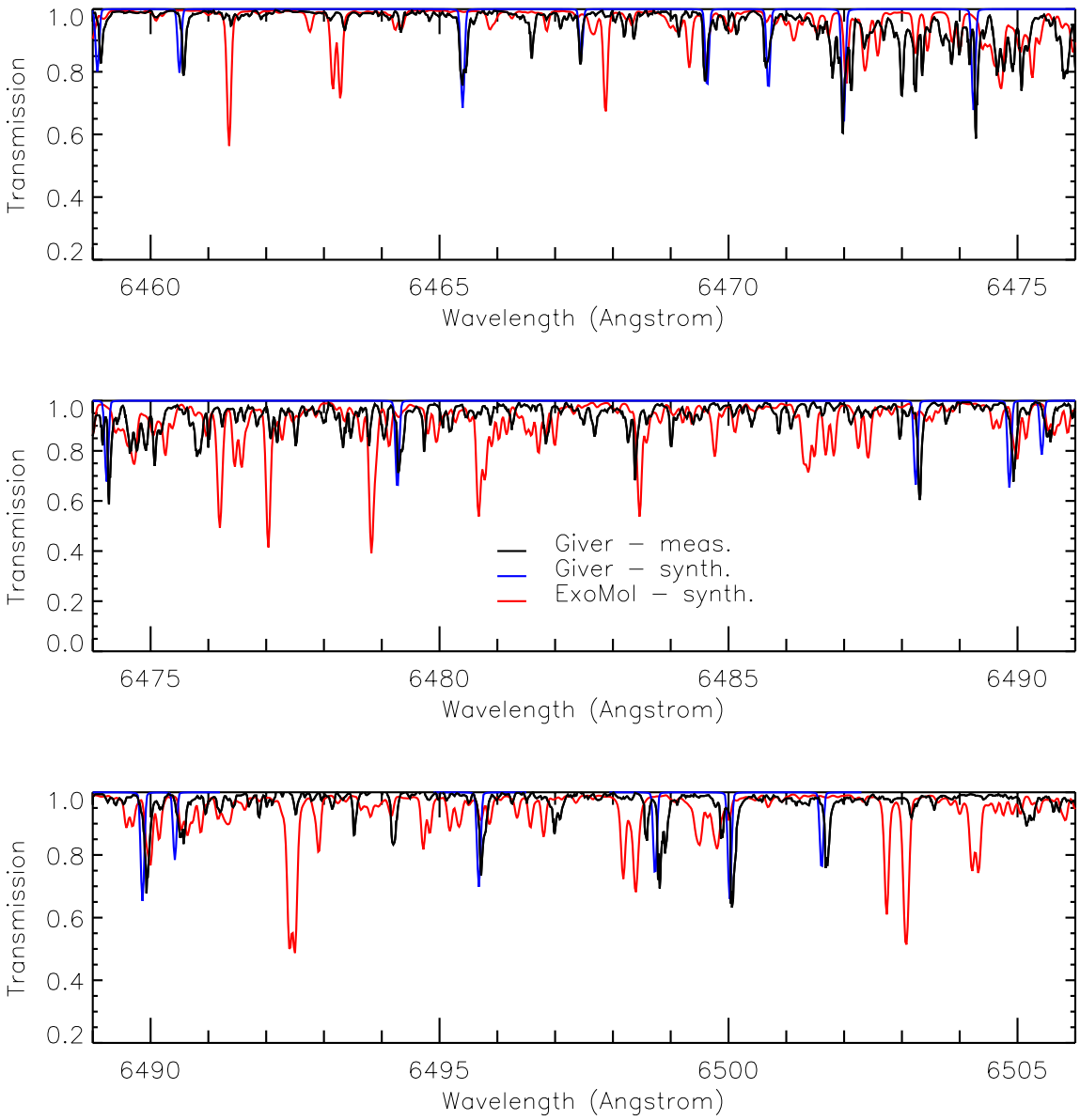

Fig. 7.— As Fig. 6, but here covering the spectral range 6460–6505 Å.

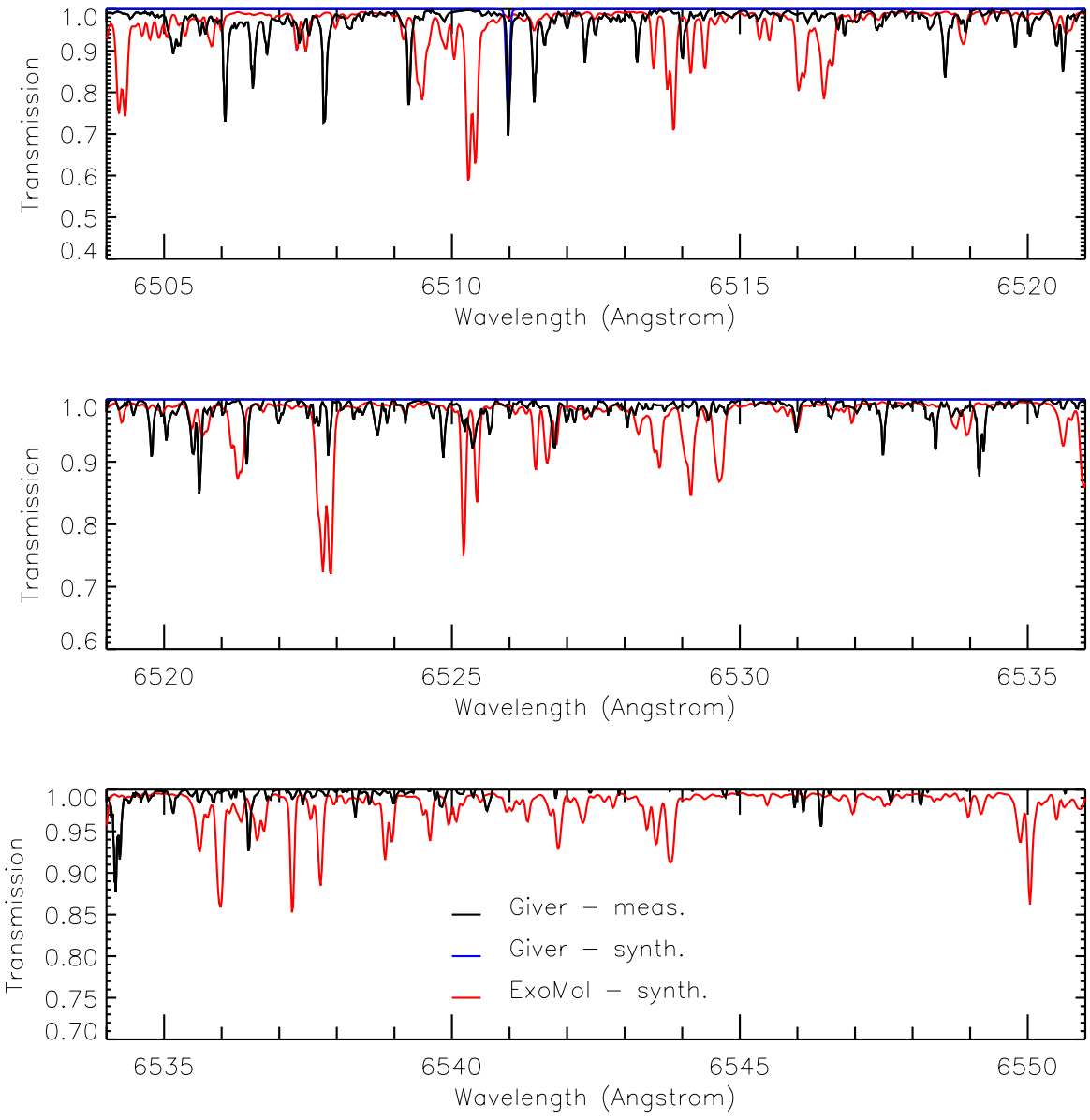

Fig. 8.— As Fig. 6, but here covering the spectral range 6505–6550 Å.

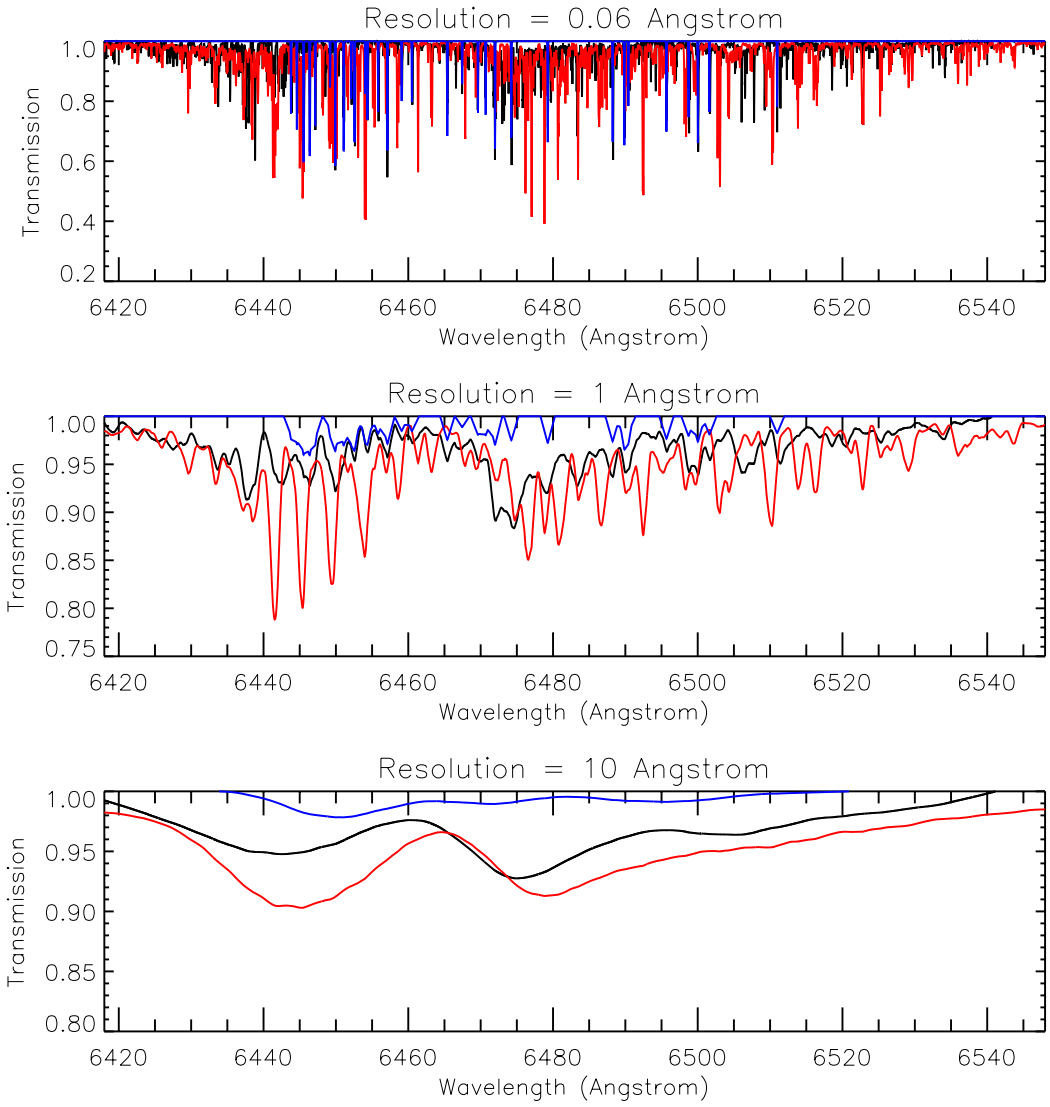

Fig. 9.— Comparison of high resolution spectra of Giver et al. (1975) covering the whole 6418 – 6548 Å range, with high spectral resolution line-by-line calculations using the line data of Giver et al. (1975) and ExoMol–C2018 (Coles et al. 2018) for the conditions specified in Fig. 1. of Giver et al. (1975), i.e. length = 400m, p = 0.061 atm, T = 294 K, and different modelled spectral resolutions (assumed triangular line shape) with FWHM = 0.06, 1.0 and 10.0 Å respectively. Here the black lines are the observed spectra in the different spectral ranges (digitised by the authors), the blue lines are the spectra calculated from the Giver et al. line data, while the red lines are the spectra calculated from the ExoMol–C2018 line data.

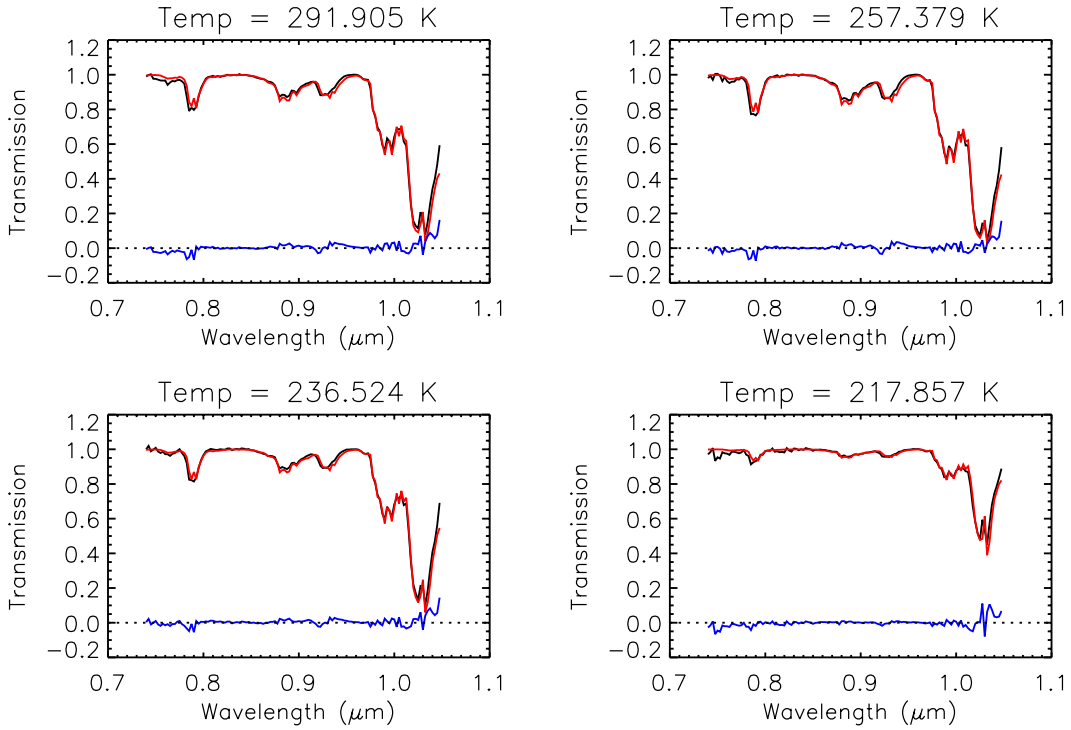

Fig. 10.— Laboratory-measured transmission spectra (black) for the longest paths observed by Bowles et al. (2008) at a range of temperatures and shown in Fig. 4 of Irwin et al. (2018), compared with spectra calculated with the ExoMol–C2018 line data (red, Coles et al. 2018) at the same resolution (0.0025 μm), and difference (blue). We can see that there is excellent correspondence and also that the spectra calculated with the C2018 line data are much less noisy than the observed spectra, particularly at the shortest wavelengths

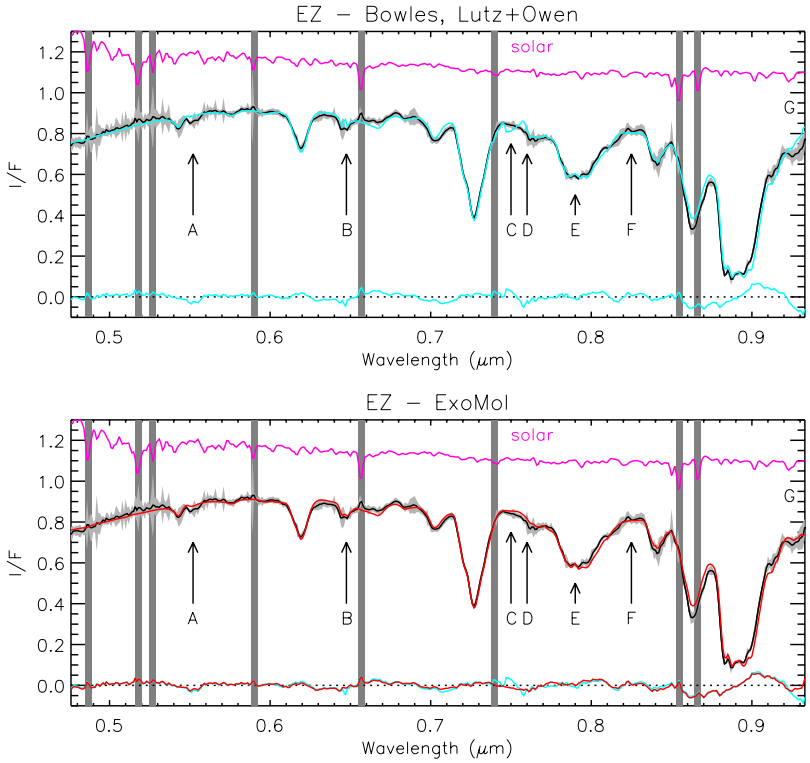

Fig. 11.— Observed MUSE spectrum taken from a single pixel in the Equatorial Zone (EZ) with estimated error (including forward model errors) shown in grey, observed on 9th April 2018 at 06:04:08UT (similar to Fig.9 of Irwin et al. (2018), which shows a fit to data from 28th May 2017). In the top panel, the cyan line is the fit of our NEMESIS retrieval model using the ammonia absorption data of Bowles et al. (2008) and Lutz and Owen (1980). In the bottom panel, the red line is the fit of our NEMESIS retrieval model using the new ExoMol–C2018 ammonia line data of Coles et al. (2018). The plots also show the differences, with the bottom plot also showing the difference (cyan) when using the previous ammonia absorption data of Bowles et al. (2008) and Lutz and Owen (1980). The labelled features 'A' to 'G' mark the main observable ammonia absorption features in the ammonia absorption data of Bowles et al. (2008) and Lutz and Owen (1980). Also shown in magenta is the assumed solar spectrum of Chance and Kurucz (2010), divided by a Planck function of temperature 5778 K and scaled to give a value of ~ 1.0, showing the various Fraunhofer lines in the spectrum, which are highlighted by the vertical grey bars.

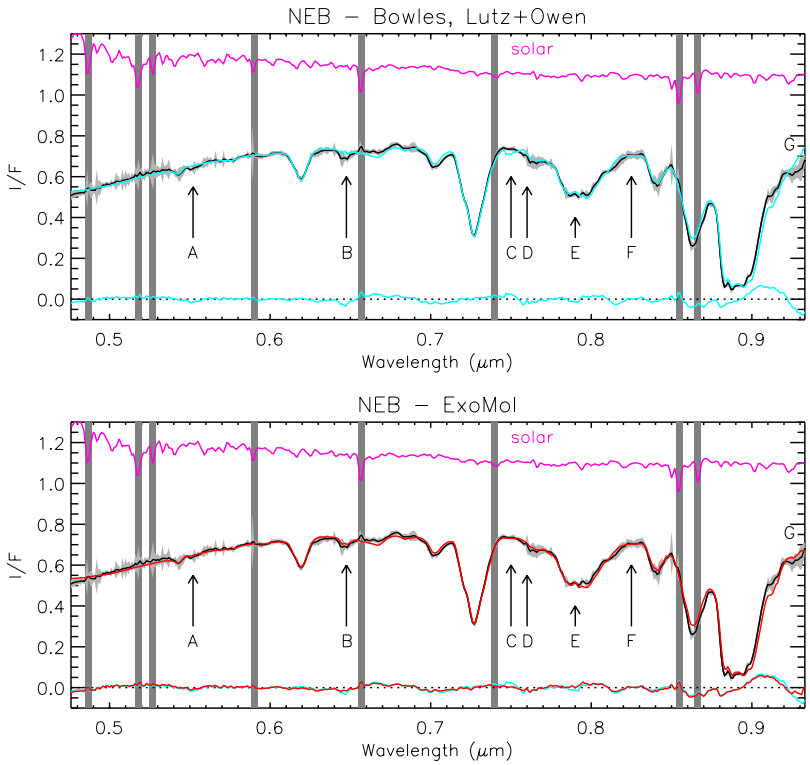

Fig. 12.— As Fig. 11, but comparing our calculations for different ammonia absorption sources with the observed MUSE spectrum in a single pixel in the North Equatorial Belt (NEB).